

Performance of the Pentagonal PdSe₂ Sheet as a Channel Material in Contact with Metal Surfaces and Graphene

Arzoo Hassan, Yaguang Guo, and Qian Wang*

Cite This: *ACS Appl. Electron. Mater.* 2020, 2, 2535–2542

Read Online

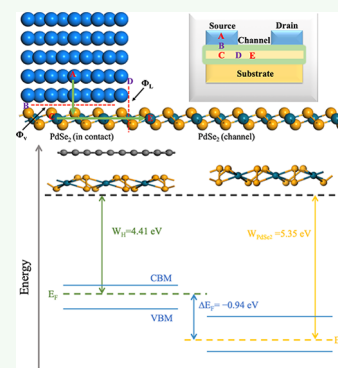
ACCESS |

Metrics & More

Article Recommendations

ABSTRACT: Motivated by the recent synthesis of the pentagonal PdSe₂ sheet [J. Am. Chem. Soc. 2017, 139, 14090], here using first-principles calculations, we have systematically carried out simulations to investigate the PdSe₂ sheet's performance as a channel material when in contact with metal surfaces and graphene. We find that the PdSe₂ sheet can almost retain its pentagonal feature with small distortions when in contact with Au(111), Ag(111), Cu(111), and Pb(111) surfaces. However, it is severely distorted on the Ti(0001) surface undergoing metallization. Band structure analysis suggests that the vertical Schottky barrier disappears in all of the metal contacts. Au, Ag, Cu, Ti, and Pb are of the Schottky type contacts with barriers of 0.62, 0.87, 0.79, 0.58, and 0.76 eV in the lateral direction for electrons, whereas both monolayer and bilayer PdSe₂ maintain their intrinsic properties when in contact with graphene forming a weak van der Waals interaction with no charge transfer between the two surfaces. Our study provides insights into selecting high-performance monolayer PdSe₂ device evaluations based on the orbital overlap, tunneling barrier, and Schottky barrier.

KEYWORDS: PdSe₂ sheet, heterojunction, Schottky barrier, density functional theory, graphene, work function



1. INTRODUCTION

Because the proposal of penta-graphene,¹ 2D structure composed of pentagons have attracted tremendous attention, such as penta-SnS₂,² penta-SnSe₂,³ penta-SnTe₂,⁴ penta-CN₂,⁵ penta-silicene,⁶ and so forth. The recently synthesized layered pentagonal PdSe₂ sheet is of special interest⁷ because of its remarkable layer-dependent electronic structure^{7,8} that goes beyond the conventional 2D transition-metal dichalcogenides (TMDs).^{9,10} “Contrary to the hexagonal phases commonly reported in layered TMDs,¹¹ PdSe₂ exhibits different bonding characteristics wherein palladium (Pd) atoms combine with four selenium (Se) atoms, forming a pentagonal network with a square backbone.¹² As explained in previous studies, the Se–Se atoms present in upper and lower planes of the PdSe₂ form a tilted dumbbell structure with Pd atoms resulting in a lack of rotational symmetry (see Figure 1). The existence of Se vacancies would disrupt the Se–Se dumbbell configuration and cause considerable structural distortion making it sensitive against defects.”¹² Sun *et al.* using first-principles calculations predicted a semiconducting behavior in PdSe₂ by studying its energy band gap, that is, 0.03 eV for the bulk phase changing to 1.43 eV for the monolayer (ML)⁸ as confirmed by optical absorption spectroscopy.⁵ “Field-effect transistors (FETs) designed by using few-layer PdSe₂ display good performance owing to its excellent properties, such as a high carrier mobility of 216–294 cm²·V⁻¹·s⁻¹ and a high on/off ratio (≈103).”^{7,13} The distinctive penta-structure and noticeable FET efficiency with exceptional atmospheric steadiness make PdSe₂ desired

and interesting for applications in electronic and photoelectric devices.^{14–17} The fabrication of FET devices using 2D materials is a hot topic currently. “Contact between the channel region and the metal electrode is needed for a high-performance 2D-FET device configuration, to induce a suitable type of charge carriers into the respective energy bands of the 2D-semiconducting channel material. In either case, realizing a low-resistant metal contact is the most significant defiance that masks the intrinsic electronic properties of a 2D-semiconductor.”²⁶ To fulfill the need for a viable doping method, it is vital to find a suitable metal substrate to contact a 2D semiconductor.

Recently, experiments showed that the fabrication of bilayer (BL) PdSe₂ could be deposited on graphene, where the interface coupling is the weak van der Waals (vdW) force.¹⁷ Thus, PdSe₂ can be separated from graphene by mechanical exfoliation and grown *via* the chemical vapor deposition method.^{7,8} Besides, the techniques to transfer 2D materials from one substrate to another are well developed.^{18,19} Therefore, we can expect that a similar method can also be applied to transfer PdSe₂ from graphene to a metal substrate.

Received: May 27, 2020

Accepted: July 23, 2020

Published: July 23, 2020



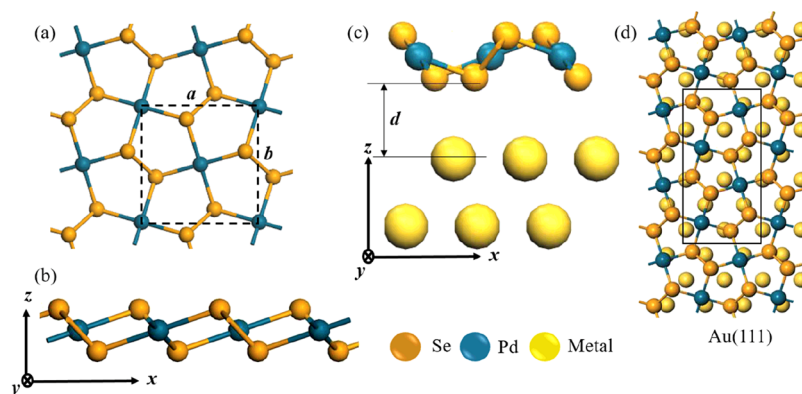


Figure 1. (a) Top view of an ML-PdSe₂ and (b) side view of an ML-PdSe₂ in 2 × 2 supercells. (c,d) Schematic diagram and top view of the PdSe₂–metal contact.

Given the application in heterojunction, PdSe₂ has been integrated into several devices such as high-yielding near-infrared photodetector based on the PdSe₂–pyramid Si heterojunction, self-powered photodetectors based on graphene–PdSe₂–germanium heterojunction, and image sensors based on the multilayer PdSe₂–perovskite Schottky junction^{20–22} with many intriguing properties such as excellent photoresponse performance, a high specific detectivity, and broadband photosensitivity attributed to the broad optical absorption properties of PdSe₂. It has also been used in the synthesis of nanowires made of the PdSe₂–Pd₂Se₃ heterojunction.²³ However, no study has been reported on the performance of PdSe₂ as a channel material in contact with metal electrodes, which prompt us to carry out this work focusing on the transport and electronic properties of the PdSe₂–metal heterojunction. For comparison, we also extend our study to the experimental synthesized PdSe₂–graphene system.

2. COMPUTATIONAL MODEL AND METHODS

Following the Schottky–Mott rule,²⁴ metals with either a large work function (WF) or minimal WF are desired to form a low-energy barrier contact reported in our previous work.²⁶ Five metals, counting silver—Ag, gold—Au, copper—Cu, chromium—Cr, lead—Pb, and titanium—Ti were selected as the contact electrode because these are usually used in transistor applications and covers a wide range of WFs.²⁵ To match the PdSe₂ ML, we choose closed pack surface (111) for Ag, Au, Pd, and Cu contacts, and (0001) surface for Ti, as these are the prevailing orientations found in other experimental and theoretical studies, and they form minimal lattice mismatch. We use a slab model to simulate the metal surfaces. A five-layer metal slab was adopted to study the film thickness effect. The bottom three metal layer's atoms are fixed at their bulk position to minimize the computational cost. We then build the heterojunctions by stacking PdSe₂ and metal surfaces vertically together forming top contacts following our previous work.²⁶ Because the lattice parameters of PdSe₂ and the chosen metal electrodes are different from each other, special care is needed to create an appropriate interface, for that, we have used our in-house code²⁶ to generate the heterojunctions. Using the code, the lattice mismatch percentage is set under 3% and the atom concentration is also under 300 to keep the lattice strain negligible. The contact regions are separated by a vacuum space of >20 Å in a path perpendicular to the interfaces to refrain the spurious interaction between the periodic images in the *x* and *y* directions.

Our simulations are based on first-principles calculation within the frame of “density functional theory (DFT), and the projector augmented wave pseudo-potential method, using Vienna *ab initio* Simulation Package.”^{21,27,28} The Perdew–Burke–Ernzerhof (PBE) functional.²⁹ “We have used a dispersion-corrected (optB88-vdW)

DFT method to describe the effect of vdW interactions correctly. The plane-wave cutoff energy is set to 500 eV for all calculations.”^{26,36} The electronic properties of the heterojunction system are calculated with 3 × 3 × 1 Monkhorst–Pack special *k*-point meshes³⁰ for Ag and Au, 5 × 9 × 1 for Cu and Ti, 5 × 5 × 1 for and Pd 9 × 5 × 1, respectively. For structural optimization, all studied heterojunctions are relaxed until the force and energy less than 0.01 eV/Å and 1 × 10^{−6} eV, respectively.²⁶

3. RESULTS AND DISCUSSION

“From the device’s point of view, the interface geometry, orbital overlap, tunneling barrier, and Schottky barrier are the four essential factors that determine the electronic transparency of the contact in a metal–semiconductor junction. We intend to acquire a small lattice mismatch for a favorable interface to increase the orbital overlap between the two surfaces. For maximum current injection, the tunneling barrier and Schottky barrier appearing at the point of contact should also be low and narrow to increase the tunneling possibility (TP) for the charge carriers and make charge transfer more efficient. In this study, the interfacial properties of PdSe₂–metal junctions are evaluated and analyzed by considering each of these factors.”²⁶

3.1. PdSe₂ Sheet with Metal Contact. The optimized atomic structure of a free-standing ML-PdSe₂ is shown in Figure 1a,b with the calculated lattice constants of *a* = 5.74 Å and *b* = 5.86 Å, which agree with experimental findings.^{7,16} The structural model of PdSe₂–metal junctions is plotted in Figure 1c. When contacting metal surfaces, the super lattice’s lattice mismatch must be carefully considered because the induced lattice strain will significantly affect the electronic properties. The pentagonal structure of PdSe₂ undergoes a distortion when coming in contact with Au, Ag, Cu, Pd, and Ti, mainly due to the strong chemical bonding at the interface. However, PdSe₂ shows negligible distortion when in contact with graphene, as the surface interaction is through the vdW force.

For heterojunctions, a critical parameter is the equilibrium separation *d* between the PdSe₂ ML and the metal surface. As listed in Table 1, the sum of the covalent radius (*d_R*) of atoms is much smaller than *d* for Ag, Au, and Pb contacts, more or less equal for the Cu contact, and much more substantial for Ti contact. Generally, *d_R* can be used to characterize the interfacial hybridization, and orbital overlap to some extent. A weak wave function overlap for *d_R* < *d* and a strong overlap for *d_R* ≫ *d*.³¹ This is evident from the fact that the shortest distance between Se on-bottom site and the listed atoms right

Table 1. Calculated Interfacial Properties of PdSe₂-Metal: *d* is the Averaged Interlayer Distance between PdSe₂-Metal Contacts, and *d_R* is the Sum of Covalent Radii^a

	Ag	Au	Cu	Ti	Pb
<i>D</i> (Å)	2.86	2.87	2.52	2.53	3.13
<i>d_R</i> (Å)	2.54	2.56	2.52	2.65	2.66
<i>E_b</i> (eV/Å ²)	0.38	0.44	0.57	1.34	0.31
Δ <i>V</i> (eV)	4.02	3.20	0	0	2.44
<i>w_B</i> (Å)	17.66	10.37	0	0	9.18
TP (%)	40	18	100	100	9.18
<i>W_H</i> (eV)	4.43	5.24	4.49	5.20	4.11
<i>W</i> (eV)	4.38	5.16	5.00	4.79	4.14
Φ _{SB-e} (eV)	0.87	0.62	0.79	0.58	0.76
Φ _{SB-h} (eV)	0.56	0.81	0.64	0.85	0.67
Δ <i>E_F</i> (eV)	0.05	0.03	-0.51	-0.14	0.41

^a*E_b* is the binding energy per unit area of the supercells. Δ*V* and *w_B* are *T_B*-height and *T_B*-width. TP represents tunneling possibility, *W* is the WF of the pure metals, and *W_H* is the WF of the heterostructure formed by the PdSe₂-metal contact. Φ_{SB-e} and Φ_{SB-h} are SBH of electron and holes in the lateral direction. Δ*E_F* is the energy difference between the Fermi levels of PdSe₂-metal heterostructure and free-standing PdSe₂ layer.

beneath it is approximately equal in the case of Cu and 0.33, 0.20, and 0.61 Å larger than the sum of covalent radii of Se and Au, Ag, and Pb (see Figures 1 and 3).²⁶

Compared to the cases of Au, Ag, and Pb, the equilibrium separation between PdSe₂ and Ti is shorter and comparable with the case Cu contact. In the former case, Se atoms in the

hollow site try to replicate Ti's environment in the stable compound TiSe₂.³² The equilibrium separation between PdSe₂ and Ti is 2.53 Å, smaller than the addition of covalent radii 2.65 Å of Ti and Se.²⁶ The average equilibrium distance between the PdSe₂-Ti interface is shorter than the rest of the three contacts, which is favorable for the wave function overlap.

To further characterize the interface coupling, we further calculate binding energy *E_b* defined as

$$E_b = (E_{\text{PdSe}_2} + E_M - E_{\text{PdSe}_2\text{-M}})/A$$

where *E_{PdSe₂}*

, *E_M*, and *E_{PdSe₂-M}* are the total energies of ML PdSe₂, the free-standing metal surface, and the corresponding heterojunction of the PdSe₂-metal system, respectively, and *A* represents the area of the supercell. The calculated *E_b* for PdSe₂-Ag, Au, Cu, Ti, and Pb junctions are 0.38, 0.44, 0.57, 1.34, and 0.31 eV/Å², respectively. According to the magnitudes of *d* and *E_b*, PdSe₂-metal interfaces can be classified into three types: weak adsorption for Pb with *E_b* = 0.31 eV/Å² and *d* = 3.13 Å; medium adsorption for Ag and Au with *E_b* = 0.38, 0.44 eV/Å² and *d* = 2.86 and 2.87 Å, respectively; strong adsorption for Cu and Ti with *E_b* = 0.57 and 1.34 eV/Å² and *d* = 2.52 and 2.53 Å, respectively.

Following, we evaluate the energy barriers at the PdSe₂-metal interface to examine the efficiency of charge transfer. The diagram of the PdSe₂-based two-probe FET prototype is shown in Figure 2. A tunneling barrier (*T_B*) can exist at the interface (B) when a charge carrier diffuse from the metal surface to the contacted ML-PdSe₂, depending on how strong

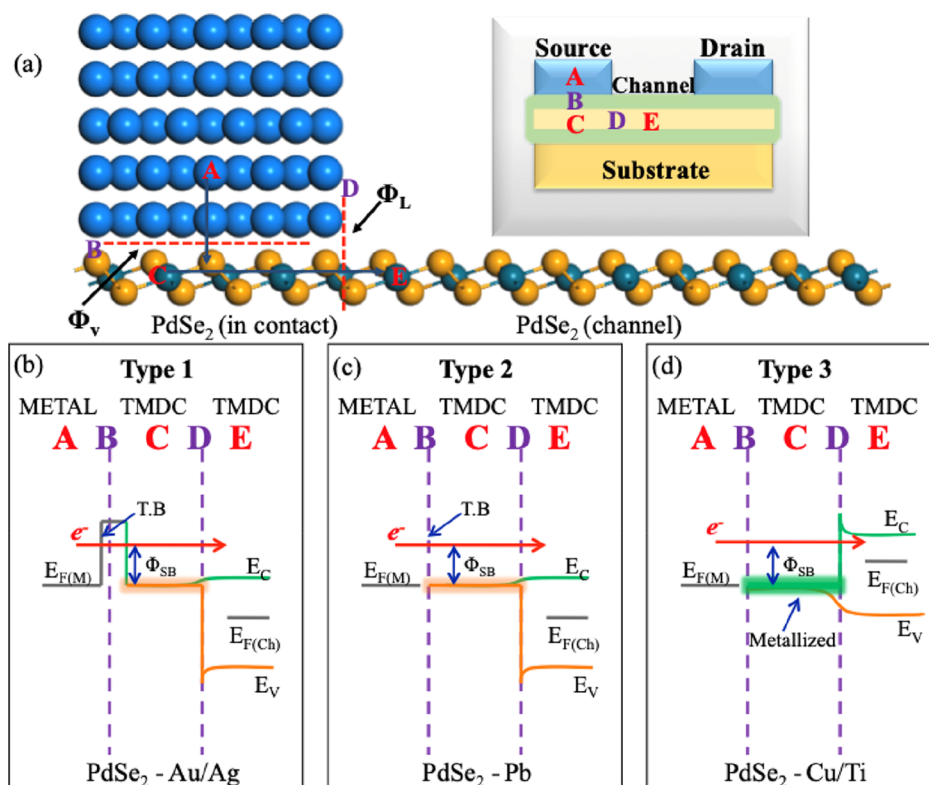


Figure 2. (a) Schematic image of a PdSe₂-metal contact. The inset shows the typical FET, with source and drain contacts and the channel region. A, C, and E denote the three regions, separated by the two interfaces B and D. The blue arrows show the pathway (A → B → C → D → E) of an electron or a hole that flows from the metal electrode to the PdSe₂ channel. Vertical and lateral Schottky barriers are denoted by Φ_V and Φ_L, respectively. (b–d) Three possible band diagrams of PdSe₂-metal contacts constructed on the evaluation of tunneling and Schottky barriers with (I) weak bonding, (II) medium bonding, and (III) strong bonding. *E_{F(M)}* and *E_{F(Ch)}* denote the Fermi level at the metal and channel regions.

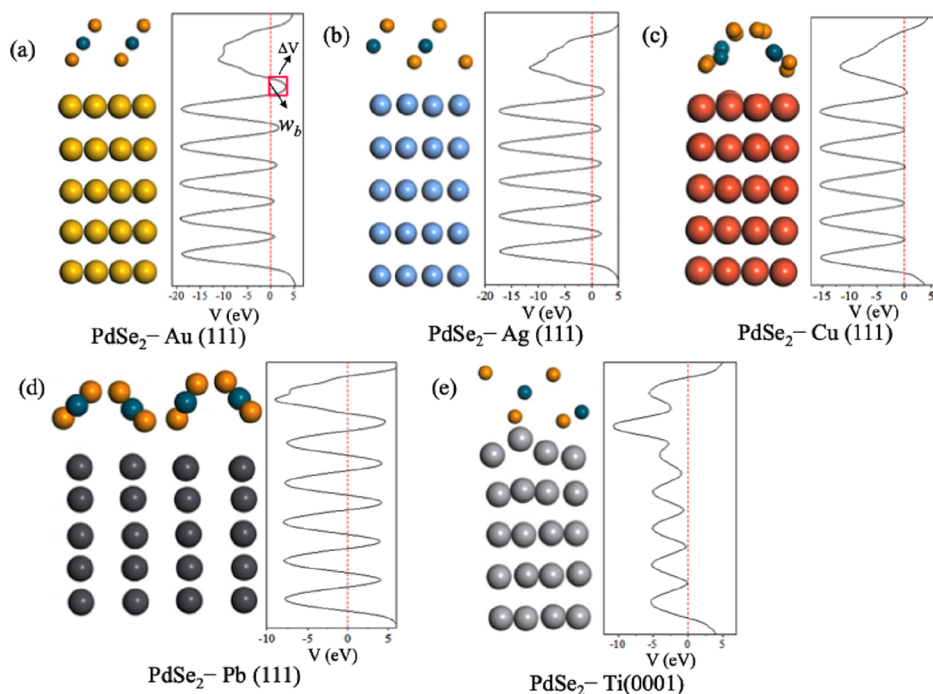


Figure 3. (a–e) Side view of the relaxed PdSe₂–Au, Ag, Cu, Pb, and Ti systems and plot of the average electrostatic potentials profiles V (eV) in the z -direction to the interfaces. ΔV and w_B are the T_B -height and T_B -width. The Fermi level is shifted to zero.

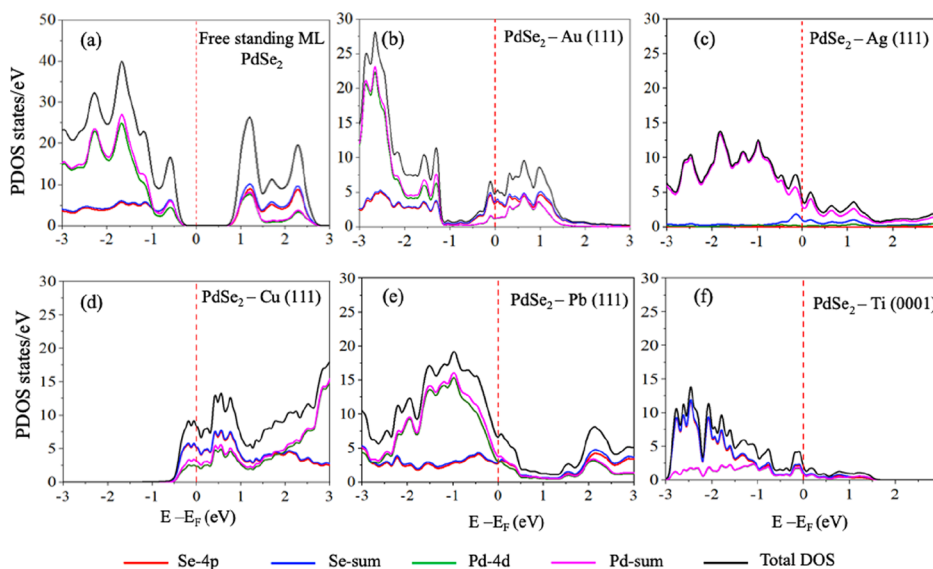


Figure 4. (a–f) PDOS of free-standing ML PdSe₂, Au, Ag, Cu, Pb, and Ti surfaces. E_F is the Fermi energy set to zero.

or weak is their binding interface. A Schottky barrier can appear at two different points one is at the interface (B) in the vertical direction, a vertical Schottky barrier (Φ_v) and the other one may appear at the interface (D) between the heterojunction and the PdSe₂ channel region called a lateral Schottky barrier (Φ_l). The tunneling barrier often exists between the 2D TMDs-metal contacts, which refer to the electrostatic potential above the Fermi level in a direction perpendicular to the interfaces. In order to evaluate the tunneling barrier first, we calculated the electrostatic potentials. From the potential profile, as shown in Figure 3, the PdSe₂–Cu and Ti contacts have no significant tunneling barriers, as their potential energies did not cross the E_F . Conversely, there is a noticeable tunneling barrier in PdSe₂–Ag, Au, and Pb with

a barrier height of 4.02, 3.20, and 2.44 eV, respectively. Because of the real potential's irregular shape, we adopt a square potential barrier (see Figure 3a) to evaluate the TP by the WKB equation^{26,33–35}

$$T_B = \exp\left(-2\frac{\sqrt{2m\Delta V}}{\hbar} \times w_B\right)$$

The tunneling barrier (T_B) can be described by its height (ΔV , the energy difference between E_F of the system and the potential energy of the interface gap) and width (w_B), m stands for the mass of the free electron, and \hbar is the reduced Planck's constant. The results show that the TP is 100% for the PdSe₂–Ti contact.

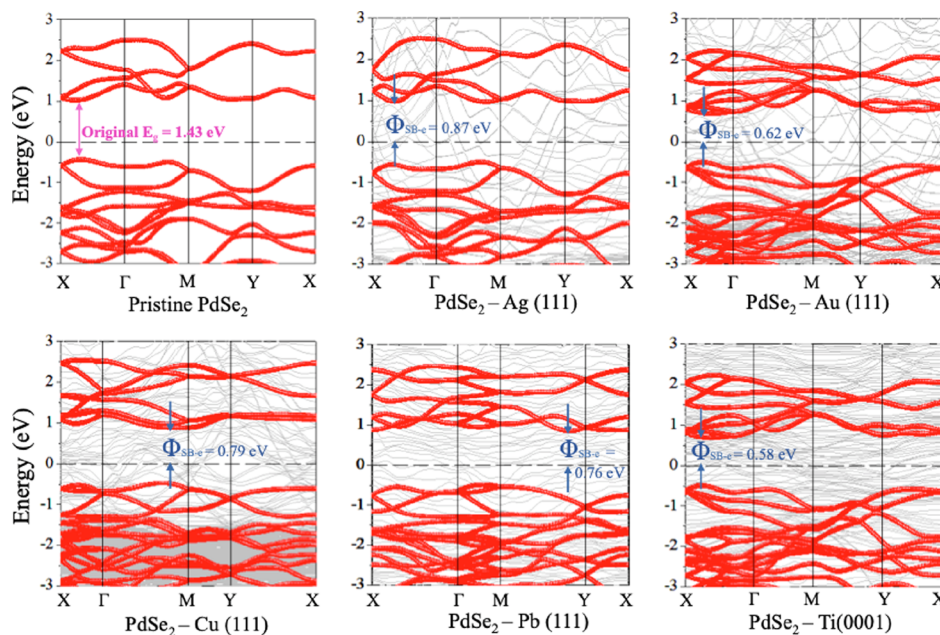


Figure 5. Band structure of free-standing PdSe₂ layer is plotted for reference (red curves), and projected band structures of PdSe₂ without contact superimposed on the new band structures (gray curves) such that the new and old sub-bands align, with the Fermi level shifted to zero energy. The Schottky barrier height (SBH) for electrons ($\Phi_{\text{SB-e}}$) is shown in blue. Because of the different dimensions of the unit cells, the symmetric points (X, Γ , M, and Y) are also different.

The density of states (DOS) projections upon selected Pd and Se orbitals are shown in Figure 4 for the free-standing ML-PdSe₂, PdSe₂-Ag, Au, Cu, Pb, and Ti systems. The band gaps disappear in all of the five systems. A significant amount of metal derived gap states appears in the original band gap of ML-PdSe₂, particularly at the Fermi level (E_{F}), resulting from the hybridization of the energy bands. As seen in Figure 4b, upon forming contact with Au, the PdSe₂-Au interface develops a metallic nature. According to Figure 4b, the flow of charge carriers will be primarily involving Se 4p states, which display a low partial DOS (PDOS) at the E_{F} . The PdSe₂-Ag interface also becomes metallic, but compared to the Au contact, it modifies the electronic states much more close to the E_{F} . There is a noteworthy role of Se 4p and Pd 4d states near the E_{F} , associated with intense Se-Ag mixing. PdSe₂-Pb also shows similar behavior; the surface becomes metalized upon contact with Pb, with modified electronic states at E_{F} . Compared to PdSe₂-Au, Ag, and Pb contacts, we can observe the significant contribution of Pd 4d states near the E_{F} for PdSe₂-Cu and Ti systems with an admixture of Se 4p states. The appearance of relatively large and broad peaks near the E_{F} for the Ag, Cu, and Pb contacts reveals an upsurge in the distribution of the related bands and suggests the development of delocalized states at the interface that allows the electron injection to PdSe₂ with a low energy barrier. In contrast, the DOS is somewhat limited at the E_{F} in other systems. Because PdSe₂ is a ML, its properties can be easily distorted because of the substantial orbital overlaps. Thus, the electronic properties of PdSe₂ with the contact change. The DOS at the Fermi level decreases in the following order: Cu > Ti > Pb > Ag > Au, which is in good agreement with the band hybridization degree (discussed in the next section).

To further confirm the metallization, the band structure analysis is carried out. In Figure 5, the energy band plots of PdSe₂-Au, Ag, Cu, Pd, and Ti systems are drawn (in gray), the original band structure of PdSe₂ (red lines) is superimposed on

new band structures (gray lines) for reference such that the former original bands and new sub-bands align. The band hybridization degree is also different for different substrates. When in contact with Cu, Pb, and Ti, both the CB (conduction band) and the VB (valance band) of PdSe₂ are significantly changed, indicate a strong band hybridization (rising from the admixture of energy bands of the metal atoms and the interfacial Se and Pd atoms), these results originate from the different partially occupied d orbitals of the metal atoms (Cu, Pb, and Ti), which form strong chemical bonds with the 4p orbital of the interfacial Se atoms and lead to intense binding energy ($E_{\text{b}} = 0.31\text{--}0.54\text{ eV/\AA}^2$). Although the metal surfaces distort the valance and CBs of PdSe₂, they are still discernible on Ag and Au. This can be understood with the following arguments: different occupied levels of metals and radius of d-orbital results in the different energy band hybridization degrees. Ag and Au have fully occupied d-orbitals, and thus hardly form covalent bonds with the 4p orbital of the interfacial Se atoms, resulting in weak binding energy ($E_{\text{b}} = 0.38, 0.44\text{ eV/\AA}^2$). Together, a significant amount of PdSe₂ bands appear in the original band gap of PdSe₂ when in contact with Ag, Au, Cu, Pb, and Ti systems (Figure 5), we conclude that PdSe₂ undergoes metallization at these surfaces; hence, the vertical Schottky barrier disappears under the metal contacts, similar to InSe-metal contact.³⁵

“Because the vertical Schottky barrier vanishes, then we calculate the Schottky barrier in the lateral direction (Φ_{L}) between the contact and the free-standing ML-PdSe₂ channel region following the same procedure as in our previous study.²⁶ SBH is defined as the energy difference between the Fermi level (E_{F}) of the heterojunction and their respective energy band edge of the semiconductor, that is, CB minimum (CBM) and VB maximum (VBM) (see Figure 5)

$$\Phi_{\text{SB-e}} = E_{\text{CBM}} - E_{\text{F}}$$

$$\Phi_{\text{SB-h}} = E_{\text{F}} - E_{\text{VBM}}$$

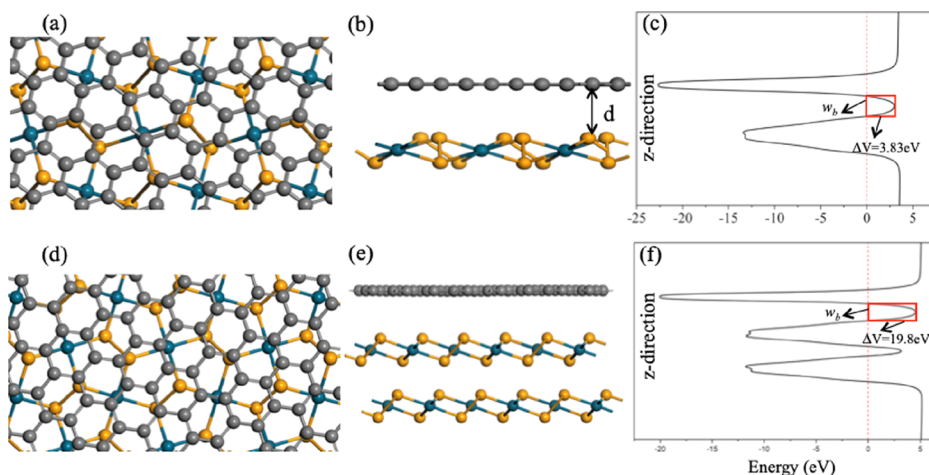


Figure 6. (a) Side and (d) Top view of ML and BL PdSe₂/graphene heterostructure, (b,e) side view of the stacked system, d represents the interlayer distance between PdSe₂ and graphene layer and, (c,f) average electrostatic potential profile in the z -direction of the interface. The red rectangular box represents the tunneling barrier, where ΔV is the tunneling barrier height, and w_b is the tunneling barrier width.

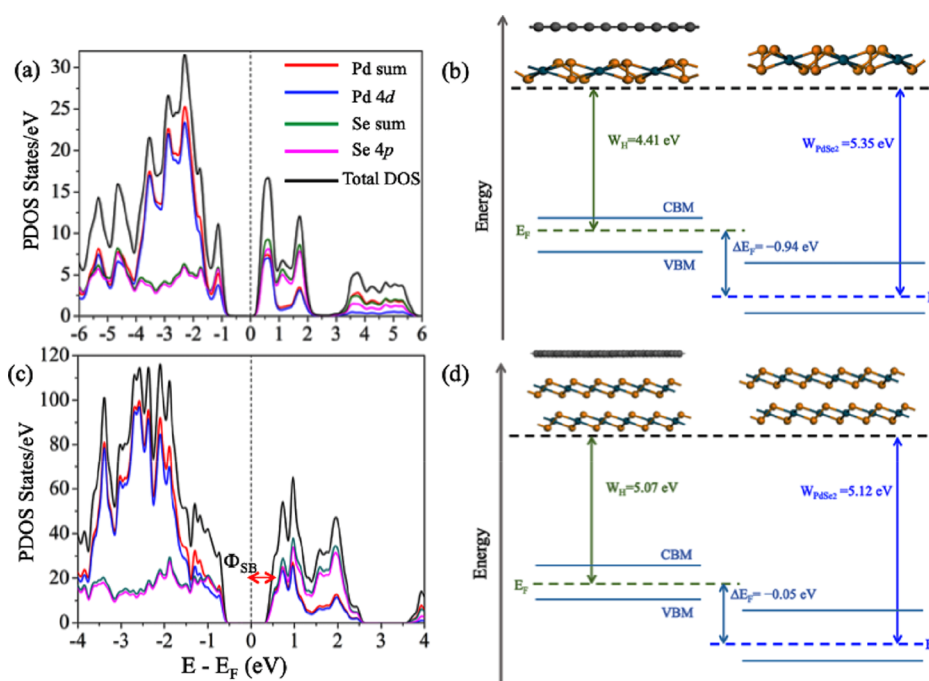


Figure 7. (a,c) Projected PDOS of PdSe₂ on ML and BL graphene, Φ_{SB} is the SBH of the contact and, (b,d) schematic description of SBH and the respective band edges of PdSe₂ on ML and BL graphene.

where Φ_{SB-e} and Φ_{SB-h} denote the lateral SBHs for electrons and holes, E_{CBM} and E_{VBM} are the energies of the CBM and the VBM of the semiconductor, respectively. Calculated values of Φ_{SB} are enlisted in Table 1. It is desired to get a low SBH (Φ_{SB-e} or Φ_{SB-h}) to minimize the contact resistance in terms of device applications. We can attain a Schottky barrier-free contact if the SBH becomes zero or negative, resulting in a spontaneous carrier infusion from the stacked system to the PdSe₂ channel. PdSe₂ forms p-type Schottky contacts with Ag, Cu, and Pb because the position of E_F of the absorbing system is shifted toward the VBM of PdSe₂, whereas it forms a n-type Schottky contact with Au and Ti, like the E_F of the absorbing system, is shifted toward the CBM of PdSe₂; thus, the conduction will be through electrons in the PdSe₂-Au and Ti heterojunction.²⁶

When considering a current-in-plane device, even without any charge transfer between PdSe₂ and metal surfaces, a small band bending can be observed. If we ignore the coupling between the heterojunction and the channel region, by definition the band bending can be obtained by the energy difference between the Fermi levels of PdSe₂-metal heterostructure and free-standing PdSe₂ layer³⁶

$$\Delta E_F = W_H - W_{PdSe_2}$$

where W_H is the WF of the heterostructure, and W_{PdSe_2} is the WF of the free-standing PdSe₂ sheet. Using the above equation, the estimated value of the band bending is -0.51 eV for the PdSe₂-Cu contact and -0.14 eV for the PdSe₂-Pb contact. As $\Delta E_F < 0$, the electrons will flow from the contacted region to the noncontacted PdSe₂ layer, making the channel

region n-type. From a device viewpoint, a smaller band bending value leads to better contact.

The summary centered on the above analysis of orbital overlap, tunneling barrier, and Schottky barrier of the contacts of PdSe₂ with metal surfaces (see Figure 2) is as follow:

- (1) Type 1 contact with Au and Ag, the latter behaves better in terms of the orbital overlap with PdSe₂, while the former is favorable in terms of SBH.
- (2) Type 2 contact with Pb, exhibiting a Schottky barrier of 0.67 eV and hence a low TP.
- (3) Type 3 contact with Cu and Ti shows a Schottky barrier of 0.58 and 0.64 eV, respectively, and no tunneling barrier at the interfaces.

3.2. PdSe₂/Graphene Heterojunction. For comparison, we carried out similar calculations for ML and BL PdSe₂ on the graphene sheet forming a heterojunction, as shown in Figure 6. Equilibrium distance d between the two sheets is 3.6 Å for the contact with the ML-PdSe₂/graphene heterojunction and 3.43 Å for the BL-PdSe₂/graphene heterojunction, leading to weak interactions (19.24 and 40.94 meV/Å²) and the features of vdW interactions, similar to other systems such as graphene/TiS₃,³⁶ graphene/WSe₂,³⁷ graphene/ZnO,³⁸ graphene/SnS,³⁹ graphene/penta-graphene,⁴⁰ and graphene/BN.⁴¹

Figure 6c,f shows the electrostatic potential profiles of ML and BL PdSe₂/graphene heterojunctions, where the irregular potential barrier is approximated with a square potential. It is evident that there exists a substantial tunneling barrier at the interface, which is also evaluated using the WKB equation, ΔV (3.83 and 19.8 eV) is more significant than that of PdSe₂-metal contacts which is consistent with the fact that a small interlayer distance between the two surfaces (heterojunction interface) usually results in low ΔV ,⁴² 3.43–3.6 Å versus 2.52–3.13 Å in this case. Moreover, the metallization of ML PdSe₂ rising from the chemical bonding with the metal surfaces can also decrease the ΔV . The existence of tunneling barrier in the PdSe₂/graphene heterojunction is similar to the cases of Au, Ag, and Pb on PdSe₂ and other TMD contacts.⁴³

To obtain the SBH of ML and BL PdSe₂/graphene heterostructure, we calculate the projected density of states on PdSe₂, as shown in Figure 7a,c. The Schottky barrier for electrons is $\Phi_{\text{SB-e}}$ of 0.22 and 0.34 eV. Both ML and BL PdSe₂/graphene heterostructures possess an n-type Φ_{SB} because the E_{F} is close to the CBM of PdSe₂. Namely, the transmission will be via electrons in the PdSe₂/graphene heterojunction. As shown in Figure 7b,d, the band bending is -0.94 , and -0.05 eV for ML and BL PdSe₂ sheet at the generalized gradient approximation-PBE level and electrons will move from the contacted region to the pristine PdSe₂ (channel region), making it n-type.

4. CONCLUSIONS

When going from hexagon-based 2D materials to pentagon-based ones, the successful synthesis of the PdSe₂ sheet becomes a milestone that validates the idea proposed in penta-graphene. To further promote the research on PdSe₂-based devices, we have studied the interfacial properties of heterojunctions formed with the PdSe₂ sheet and Ag, Au, Cu, Pb, Ti, and graphene electrodes by using *ab initio* electronic structure calculations in a FET environment. We have found strong interactions between ML-PdSe₂ and all the selected metal electrodes on the point of contact, whereas ML-PdSe₂ forms a vdW interaction with graphene. Therefore, the

band structure of PdSe₂ significantly changes under the contact of all the checked metals. Especially, the ML-PdSe₂ sheet forms n-type Schottky contacts with Au, Ti, and graphene electrodes having electron SBH of 0.62, 0.58, 0.22 eV (ML), and 0.34 eV (BL) PdSe₂/graphene heterojunction, respectively. Ag, Cu, and Pb electrodes form p-type Schottky contacts with hole SBHs of 0.56, 0.64, and 0.67 eV, showing flexibility in tuning the device performance with different electrodes.

■ AUTHOR INFORMATION

Corresponding Author

Qian Wang – Center for Applied Physics and Technology, Department of Materials Science and Engineering, HEDPS, BKL-MEMD, College of Engineering, Peking University, Beijing 100871, China; orcid.org/0000-0002-9766-4617; Email: qianwang2@pku.edu.cn

Authors

Arzoo Hassan – Center for Applied Physics and Technology, Department of Materials Science and Engineering, HEDPS, BKL-MEMD, College of Engineering, Peking University, Beijing 100871, China

Yaguang Guo – Center for Applied Physics and Technology, Department of Materials Science and Engineering, HEDPS, BKL-MEMD, College of Engineering, Peking University, Beijing 100871, China

Complete contact information is available at: <https://pubs.acs.org/10.1021/acsaelm.0c00438>

Notes

The authors declare no competing financial interest.

■ ACKNOWLEDGMENTS

This work is partially supported by grants from the National Natural Science Foundation of China (grant nos. 21773004 and 11974028), the National Key Research and Development Program of the Ministry of Science and Technology of China (grants no. 2017YFA0205003), and is supported by the High-Performance Computing Platform of Peking University, China. Y.G. acknowledges the Project funded by China Postdoctoral Science Foundation (no. 2019M650289).

■ REFERENCES

- (1) Zhang, S.; Zhou, J.; Wang, Q.; Chen, X.; Kawazoe, Y.; Jena, P. Penta-Graphene: A New Carbon Allotrope. *Proc. Natl. Acad. Sci. U.S.A.* **2015**, *112*, 2372.
- (2) Shrividhya, T.; Ravi, G.; Mahalingam, T. Electrosynthesis of SnS Thin Films with Pentagon Hallow like Architectures. *Int. J. ChemTech Res.* **2014**, *6*, 3382–3384.
- (3) Ma, Y.; Kou, L.; Li, X.; Dai, Y.; Heine, T. Room Temperature Quantum Spin Hall States in Two-Dimensional Crystals Composed of Pentagonal Rings and Their Quantum Wells. *NPG Asia Mater.* **2016**, *8*, No. e264.
- (4) Zhang, R.-W.; Liu, C.-C.; Ma, D.-S.; Yao, Y. From Node-Line Semimetals to Large-Gap Quantum Spin Hall States in a Family of Pentagonal Group-IVA Chalcogenide. *Phys. Rev. B* **2018**, *97*, 125312.
- (5) Zhang, S.; Zhou, J.; Wang, Q.; Jena, P. Beyond Graphitic Carbon Nitride: Nitrogen-Rich Penta-CN₂ Sheet. *J. Phys. Chem. C* **2016**, *120*, 3993–3998.
- (6) Guo, Y.; Wang, Q. An Elemental Ferroelectric Material with High Curie Temperature. *Bulletin of the American Physical Society*, 2020; Vol. 65.
- (7) Oyedele, A. D.; Yang, S.; Liang, L.; Puzetzy, A. A.; Wang, K.; Zhang, J.; Yu, P.; Pudasaini, P. R.; Ghosh, A. W.; Liu, Z.; Rouleau, C.

- M.; Sumpter, B. G.; Chisholm, M. F.; Zhou, W.; Rack, P. D.; Geohegan, D. B.; Xiao, K. PdSe₂: Pentagonal Two-Dimensional Layers with High Air Stability for Electronics. *J. Am. Chem. Soc.* **2017**, *139*, 14090–14097.
- (8) Gu, Y.; Cai, H.; Dong, J.; Yu, Y.; Hoffman, A. N.; Liu, C.; Oyedele, A. D.; Lin, Y. C.; Ge, Z.; Puzos, A. A.; Duscher, G.; Chisholm, M. F.; Rack, P. D.; Rouleau, C. M.; Gai, Z.; Meng, X.; Ding, F.; Geohegan, D. B.; Xiao, K. Two-Dimensional Palladium Diselenide with Strong In-Plane Optical Anisotropy and High Mobility Grown by Chemical Vapor Deposition. *Adv. Mater.* **2020**, *32*, 1906238.
- (9) Sun, J.; Shi, H.; Siegrist, T.; Singh, D. J. Electronic, Transport, and Optical Properties of Bulk and Mono-Layer PdSe₂. *Appl. Phys. Lett.* **2015**, *107*, 153902.
- (10) Kan, M.; Wang, B.; Lee, Y. H.; Sun, Q. A Density Functional Theory Study of the Tunable Structure, Magnetism, and Metal-Insulator Phase Transition in VS₂ Monolayers Induced by in-Plane Biaxial Strain. *Nano Res.* **2015**, *8*, 1348–1356.
- (11) Kan, M.; Nam, H. G.; Lee, Y. H.; Sun, Q. Phase Stability and Raman Vibration of the Molybdenum Ditelluride (MoTe₂) Monolayer. *Phys. Chem. Chem. Phys.* **2015**, *17*, 14866–14871.
- (12) Chhowalla, M.; Shin, H. S.; Eda, G.; Li, L.-J.; Loh, K. P.; Zhang, H. The Chemistry of Two-Dimensional Layered Transition Metal Dichalcogenide Nanosheets. *Nat. Chem.* **2013**, *5*, 263.
- (13) Souillard, C.; Rocquefelte, X.; Petit, P.-E.; Evain, M.; Jobic, S.; Itié, J.-P.; Munsch, P.; Koo, H.-J.; Whangbo, M.-H. Experimental and Theoretical Investigation on the Relative Stability of the PdS₂- and Pyrite-Type Structures of PdSe₂. *Inorg. Chem.* **2004**, *43*, 1943–1949.
- (14) Elghazali, M. A.; Naumov, P. G.; Mirhosseini, H.; Süß, V.; Mücklich, L.; Schnelle, W.; Felser, C.; Medvedev, S. A. Pressure-Induced Superconductivity up to 13.1 K in the Pyrite Phase of Palladium Diselenide PdS₂. *Phys. Rev. B* **2017**, *96*, 060509.
- (15) Lei, W.; Zhang, S.; Heymann, G.; Tang, X.; Wen, J.; Zheng, X.; Hu, G.; Ming, X. A New 2D High-Pressure Phase of PdSe₂ with High-Mobility Transport Anisotropy for Photovoltaic Applications. *J. Mater. Chem. C* **2019**, *7*, 2096–2105.
- (16) Luo, L. B.; Wang, D.; Xie, C.; Hu, J. G.; Zhao, X. Y.; Liang, F. X. PdSe₂ Multilayer on Germanium Nanocones Array with Light Trapping Effect for Sensitive Infrared Photodetector and Image Sensing Application. *Adv. Funct. Mater.* **2019**, *29*, 1900849.
- (17) Li, E.; Wang, D.; Fan, P.; Zhang, R.; Zhang, Y.-Y.; Li, G.; Mao, J.; Wang, Y.; Lin, X.; Du, S.; Gao, H.-J. Construction of Bilayer PdSe₂ on Epitaxial Graphene. *Nano Res.* **2018**, *11*, 5858–5865.
- (18) Unarunotai, S.; Murata, Y.; Chialvo, C. E.; Kim, H.-s.; MacLaren, S.; Mason, N.; Petrov, I.; Rogers, J. A. Transfer of Graphene Layers Grown on SiC Wafers to Other Substrates and Their Integration into Field Effect Transistors. *Appl. Phys. Lett.* **2009**, *95*, 202101.
- (19) Reina, A.; Son, H.; Jiao, L.; Fan, B.; Dresselhaus, M. S.; Liu, Z.; Kong, J. Transferring and Identification of Single- and Few-Layer Graphene on Arbitrary Substrates. *J. Phys. Chem. C* **2008**, *112*, 17741.
- (20) Liang, F.-X.; Zhao, X.-Y.; Jiang, J.-J.; Hu, J.-G.; Xie, W.-Q.; Lv, J.; Zhang, Z.-X.; Wu, D.; Luo, L.-B. Light Confinement Effect Induced Highly Sensitive, Self-Driven Near-Infrared Photodetector and Image Sensor Based on Multilayer PdSe₂/Pyramid Si Heterojunction. *Small* **2019**, *15*, 1903831.
- (21) Wu, D.; Guo, J.; Du, J.; Xia, C.; Zeng, L.; Tian, Y.; Shi, Z.; Tian, Y.; Li, X. J.; Tsang, Y. H.; Jie, J. Highly Polarization-Sensitive, Broadband, Self-Powered Photodetector Based on Graphene/PdSe₂/Germanium Heterojunction. *ACS Nano* **2019**, *13*, 9907–9917.
- (22) Zeng, L.-H.; Chen, Q.-M.; Zhang, Z.-X.; Wu, D.; Yuan, H.; Li, Y.-Y.; Qarony, W.; Lau, S. P.; Luo, L. B.; Tsang, Y. H. Multilayered PdSe₂/Perovskite Schottky Junction for Fast, Self-Powered, Polarization-Sensitive, Broadband Photodetectors, and Image Sensor Application. *Adv. Sci.* **2019**, *6*, 1901134.
- (23) Zuluaga, S.; Lin, J.; Suenaga, K.; Pantelides, S. T. Two-Dimensional PdSe₂-Pd₂Se₃ Junctions Can Serve as Nanowires. *2D Mater.* **2018**, *5*, 035025.
- (24) Blom, P. W. M.; Wolf, R. M.; Cillessen, J. F. M.; Krijn, M. P. C. M. Ferroelectric Schottky Diode. *Phys. Rev. Lett.* **1994**, *73*, 2107.
- (25) Skriver, H. L.; Rosengaard, N. M. Surface Energy and Work Function of Elemental Metals. *Phys. Rev. B: Condens. Matter Mater. Phys.* **1992**, *46*, 7157.
- (26) Hassan, A.; Guo, Y.; Wang, Q.; Kawazoe, Y.; Jena, P. Interfacial Properties of Penta-Graphene-Metal Contacts. *J. Appl. Phys.* **2019**, *125*, 065308.
- (27) Kresse, G.; Joubert, D. From Ultrasoft Pseudopotentials to the Projector Augmented-Wave Method. *Phys. Rev. B: Condens. Matter Mater. Phys.* **1999**, *59*, 1758.
- (28) Blöchl, P. E. Projector Augmented-Wave Method. *Phys. Rev. B: Condens. Matter Mater. Phys.* **1994**, *50*, 17953.
- (29) Perdew, J. P.; Burke, K.; Ernzerhof, M. Generalized Gradient Approximation Made Simple. *Phys. Rev. Lett.* **1996**, *78*, 3865.
- (30) Monkhorst, H. J.; Pack, J. D. Special Points for Brillouin-Zone Integrations. *Phys. Rev. B: Solid State* **1976**, *13*, 5188.
- (31) Popov, I.; Seifert, G.; Tománek, D. Designing Electrical Contacts to MoS₂ Monolayers: A Computational Study. *Phys. Rev. Lett.* **2012**, *108*, 156802.
- (32) Di Salvo, F. J.; Moncton, D. E.; Waszczak, J. V. Electronic Properties and Superlattice Formation in the Semimetal TiSe₂. *Phys. Rev. B: Solid State* **1976**, *14*, 4321.
- (33) Pan, Y.; Wang, Y.; Ye, M.; Quhe, R.; Zhong, H.; Song, Z.; Peng, X.; Yu, D.; Yang, J.; Shi, J.; Lu, J. Monolayer Phosphorene-Metal Contacts. *Chem. Mater.* **2016**, *28*, 2100–2109.
- (34) Ji, X.; Zhang, J.; Wang, Y.; Qian, H.; Yu, Z. A Theoretical Model for Metal-Graphene Contact Resistance Using a DFT-NEGF Method. *Phys. Chem. Chem. Phys.* **2013**, *15*, 17883–17886.
- (35) Xu, L.; Pan, Y.; Liu, S.; Shi, B.; Xu, L.; Yang, J.; Yan, J.; Pang, H.; Zhang, X.; Yang, C.; Yang, J.; Wang, Y.; Zhang, Z.; Lu, J. Computational Study of Ohmic Contact at Bilayer InSe-Metal Interfaces: Implications for Field-Effect Transistors. *ACS Appl. Nano Mater.* **2019**, *2*, 6898–6908.
- (36) Liu, J.; Guo, Y.; Wang, F. Q.; Wang, Q. TiS₃ Sheet Based van Der Waals Heterostructures with a Tunable Schottky Barrier. *Nanoscale* **2018**, *10*, 807–815.
- (37) Lin, Y.-C.; Chang, C.-Y. S.; Ghosh, R. K.; Li, J.; Zhu, H.; Addou, R.; Diaconescu, B.; Ohta, T.; Peng, X.; Lu, N.; Kim, M. J.; Robinson, J. T.; Wallace, R. M.; Mayer, T. S.; Datta, S.; Li, L.-J.; Robinson, J. A. Atomically Thin Heterostructures Based on Single-Layer Tungsten Diselenide and Graphene. *Nano Lett.* **2014**, *14*, 6936–6941.
- (38) Geng, W.; Zhao, X.; Liu, H.; Yao, X. Influence of Interface Structure on the Properties of ZnO/Graphene Composites: A Theoretical Study by Density Functional Theory Calculations. *J. Phys. Chem. C* **2013**, *117*, 10536–10544.
- (39) Xiong, W.; Xia, C.; Zhao, X.; Wang, T.; Jia, Y. Effects of Strain and Electric Field on Electronic Structures and Schottky Barrier in Graphene and SnS Hybrid Heterostructures. *Carbon* **2016**, *109*, 737–746.
- (40) Guo, Y.; Wang, F. Q.; Wang, Q. An All-Carbon VdW Heterojunction Composed of Penta-Graphene and Graphene: Tuning the Schottky Barrier by Electrostatic Gating or Nitrogen Doping. *Appl. Phys. Lett.* **2017**, *111*, 073503.
- (41) Zhang, C.; Zhao, S.; Jin, C.; Koh, A. L.; Zhou, Y.; Xu, W.; Li, Q.; Xiong, Q.; Peng, H.; Liu, Z. Direct Growth of Large-Area Graphene and Boron Nitride Heterostructures by a Co-Segregation Method. *Nat. Commun.* **2015**, *6*, 6519.
- (42) Kang, J.; Liu, W.; Sarkar, D.; Jena, D.; Banerjee, K. Computational Study of Metal Contacts to Monolayer Transition-Metal Dichalcogenide Semiconductors. *Phys. Rev. X* **2014**, *4*, 031005.
- (43) Azizi, A.; Eichfeld, S.; Geschwind, G.; Zhang, K.; Jiang, B.; Mukherjee, D.; Hossain, L.; Piasecki, A. F.; Kabius, B.; Robinson, J. A.; Alem, N. Freestanding van Der Waals Heterostructures of Graphene and Transition Metal Dichalcogenides. *ACS Nano* **2015**, *9*, 4882–4890.